2.4 The complexities of thunderstorm avoidance due to turbulence and implications for traffic flow management

Robert D. Sharman* and John K. Williams
National Center for Atmospheric Research, Boulder, Colorado

ABSTRACT

Managing traffic flow in the vicinity of thunderstorms has traditionally been accomplished by avoidance, based in part on FAA guidelines that establish safety buffers around and over thunderstorms. However, recent advances in our understanding of out-of-cloud convectively-induced turbulence (CIT) processes have pointed to deficiencies in these guidelines, and the need for their revision. This paper will review case studies of turbulence encounters near cloud and statistical analyses of the relation of turbulence levels to radar-derived cloud boundaries. It is shown that the CIT formation process is complex, and often due to processes in which the storm significantly modifies its environment. The CIT prediction problem is complicated by the fact that some of these processes may be subgrid-scale relative to standard numerical weather prediction (NWP) model resolutions. Given this state of affairs, avoidance guidelines must necessarily be situationally dependent and probabilistic, and could only be reliably provided by automated real-time CIT diagnostic (DCIT) and prediction tools. In the context of air traffic route management, these CIT prediction tools may be used to make routing decisions that minimize the probability of encountering elevated turbulence regions both within and outside the cloud. In particular, future automated traffic flow management (TFM) systems must account for turbulence hazards within, above and around thunderstorms when determining routes.

1. INTRODUCTION

Convectively-induced turbulence (CIT) is one of several threats that requires aircraft to avoid thunderstorms in order to mitigate the risk of passenger injury or aircraft damage. Current Federal Aviation Administration (FAA) thunderstorm avoidance guidelines proscribe flight within 20 nautical miles of a thunderstorm, above thunderstorm tops or beneath anvils. In practice, interpretation of these guidelines is subjective and limited by available weather information, and the guidelines may make large regions of airspace unavailable to aircraft on days of widespread convection. An automated turbulence product that makes use of radar, lightning, satellite, numerical weather model and convective nowcast data to objectively diagnose the likelihood of turbulence both within the cloud and in the near-storm environment could provide valuable strategic and tactical decision support to pilots, dispatchers and air traffic controllers.

To support the next-generation air transportation system (NextGen) goals of dramatically increasing air traffic capacity within the next 20 years, it is necessary to better understand and predict the turbulence hazard associated with thunderstorms, both within and outside the cloud, to allow for better routing decisions in the vicinity of the thunderstorms. Ultimately, these decisions will be made by automated traffic flow management (TFM) tools that will consider turbulence as well as other aviation hazards. Routing efficiency and hazard tradeoffs will have to be made, and it could be that in many cases it may in fact be safer to penetrate thunderstorm clouds of known turbulence locations and intensities rather than to try to circumnavigate the storm cell or complex. This paper reviews current and future detection and nowcast CIT products that can be used to identify the location and intensity turbulence both within and surrounding thunderstorms, which is a necessary ingredient for TFM models.

2. THE CIT AVOIDANCE PROBLEM

CIT in and around thunderstorms has been shown to be responsible for over 60% of turbulence-related aircraft accidents (Cornman and Carmichael 1993; see also Kaplan et al. 2005). Accurate diagnosis of this important source of turbulence will improve airline safety and also help mitigate the significant delays that now frequently afflict the national airspace system during periods of widespread convection.

The mechanisms for the generation and propagation of CIT are not currently well-understood by researchers. As the FAA thunderstorm avoidance guidelines indicate, CIT is commonly thought to be related to the proximity (vertical and horizontal), intensity, depth and extent of convection. The guidelines include the following:

- *Don't attempt to fly under a thunderstorm even if you can see through to the other side. Turbulence and wind shear under the storm could be disastrous.*
- *Do avoid by at least 20 miles any thunderstorm identified as severe or giving an intense radar echo. This is especially true under the anvil of a large cumulonimbus.*
- *Do clear the top of a known or suspected severe thunderstorm by at least 1,000 feet altitude for each 10 knots of wind speed at the cloud top.*

* *Corresponding author address:* Dr. Robert Sharman, National Center for Atmospheric Research, Research Applications Laboratory, Boulder, CO 80307; email: sharman@ucar.edu.

- *Do circumnavigate the entire area if the area has 6/10 thunderstorm coverage.*
- *Do regard as extremely hazardous any thunderstorm with tops 35,000 ft. or higher whether the top is visually sighted or determined by radar.*

(source: FAA Advisory Circular 00-24, available at www.airweb.faa.gov/Regulatory_and_Guidance_Library /rgAdvisoryCircular.nsf/, and FAA Aeronautical Information Manual section 7-1-30, available from www.faa.gov/atpubs/AIM/). Investigations based on case studies and high-resolution numerical simulations (e.g., Lane and Sharman 2008; Fovell et al. 2007; Trier and Sharman 2009) have shown these guidelines to be inadequate and to grossly oversimplify the environments that can lead to hazardous turbulence surrounding thunderstorms. Nevertheless, our current understanding is still inadequate to provide better general-purpose "guidelines". The approach that makes more sense is to provide users with guidance based on real-time observations of turbulence in and around cloud together with indicators that are being developed by the research community that better predict out-of-cloud CIT events based on a number of environmental and storm features.

3. CIT DIAGNOSIS

A reliable CIT detection and nowcast procedure must combine accurate quantitative observations of turbulence in and around cloud with other relevant information about the cloud environment and storm properties that may be conducive to out-of-cloud CIT. An FAA and NASA-funded effort is underway to use thunderstorm features derived from various observations and numerical weather prediction (NWP) model data representing the storm environment to infer locations in and around storms where turbulence is likely to exist. The new CIT diagnosis product resulting from this research, called DCIT, will be incorporated into a new "nowcast" version of the FAA-sponsored Graphical Turbulence Guidance (GTG) turbulence forecast product (Sharman et al. 2006b), dubbed GTGN (for GTG Nowcast). Consequently there are four active research areas associated with the test and development of the DCIT product: (1) obtaining accurate, quantitative *in situ* measurements of turbulence in and around cloud, (2) accurate, quantitative, and timely remote sensing of turbulence in cloud, (3) statistical studies of correlations of CIT with NWP model fields that may be indicative of turbulence ("turbulence diagnostics"), and (4) case studies of observed CIT using high-resolution numerical simulations with the goal of better understanding the cause of the CIT, which should allow development of more reliable CIT diagnostics.

a. In situ observations

Real-time observations in the form of pilot reports (PIREPs) are inadequate to monitor CIT encounters because of the large time and position uncertainties associated with these reports (Wolff and Sharman 2008). Instead turbulence observations must be supplied with the new *in situ* turbulence measurements (Cornman et al. 1995, Cornman et al. 2004, Sharman et al. 2006a) now available from some airlines (viz., United Airlines B-737 and B-757 aircraft and Delta Airlines B-737-800 aircraft). These reports have positional accuracy better than 15 km and time accuracies of at least 1 min., and are therefore well-suited for case studies and statistical studies of CIT. The *in situ* turbulence measurement and recording system provides reports of eddy dissipation rate (EDR, $\varepsilon^{1/3}$), an aircraft-independent atmospheric turbulence metric, at approximately one-minute intervals, including both the median and 90th percentile ("peak") EDR encountered over that period. The United EDR data are reported in bins centered at 0.05 (roughly, null turbulence), 0.15 and 0.25 (light turbulence), 0.35 and 0.45 (moderate turbulence), 0.55 and 0.65 (severe turbulence), and 0.75 $m^{2/3}$ s^{-1} (extreme turbulence). The present study utilizes the peak EDR value because it supplies a good indication of hazard to the aircraft and is better distributed over the reporting bins. The location of each aircraft EDR report is taken to be the midpoint of each 1-minute flight segment; since commercial aircraft typically fly at airspeeds near 250 m s^{-1}, the peak EDR locations may be in error by 4 nmi (7.4 km) or more. Nevertheless, these uncertainties are significantly less than those of PIREPs, and the high temporal and spatial resolution and objective nature of the *in situ* EDR reports make them ideal for the present study.

To gain a better understanding of the frequency of occurrence of CIT relative to cloud reflectivity boundaries, *in situ* EDR data was compared to cloud proximity based using over 12 million reports from the summers of 2004 and 2005. Figure depicts the distribution of distances (in nmi) to convection having vertically-integrated liquid (VIL) above 3.5 kg m^{-2} for each of several levels of measured peak EDR ranging from light to severe turbulence categories. The *z*-axis is normalized to show the turbulence "relative risk", that is, the frequency of that level of turbulence divided by its overall frequency in the dataset. The increasing risk of turbulence encounters as the aircraft nears the thunderstorm is clearly evident, and shows that the risk of severe turbulence is twice the background value as far away is 40 nmi from the storm. Figure 2 depicts the distribution of turbulence encounters as a function of the aircraft's distance above the NEXRAD echo top; negative values represent encounters below the echo top. Again, there is a clearly more turbulence of all levels within the cloud than above it, and the relative risk of severe turbulence is still five times the background value as much as 10,000 ft above the echo top.

b. In-cloud turbulence measurements (NTDA)

Real-time observations of turbulence in cloud are available from the NEXRAD Turbulence Detection Algorithm (NTDA; Williams et al. 2008). The NTDA has been developed at NCAR during the past several years under direction and funding from the FAA's Aviation Weather Research Program (AWRP) with the goal of using the nation's network of operational Doppler

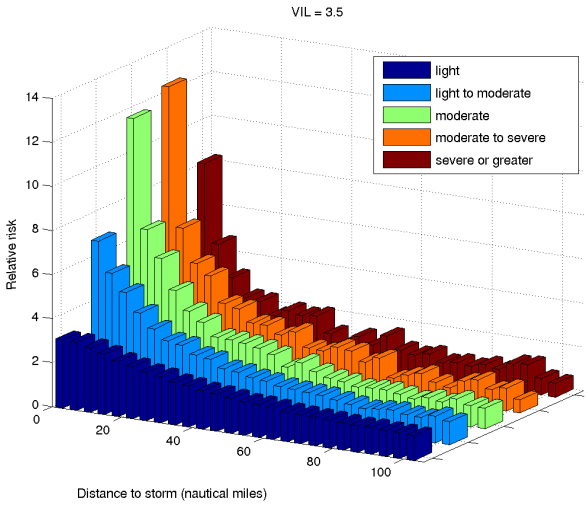

Figure 1: Distribution of distances to convection having VIL > 3.5 kg m^{-2} for various levels of peak EDR (dark blue = 0.15, light blue = 0.25, green = 0.35, orange = 0.45, and dark red = 0.55 or greater). The *z*-axis is normalized to show "relative risk", that is, the frequency of that level of turbulence divided by its overall frequency in the dataset.

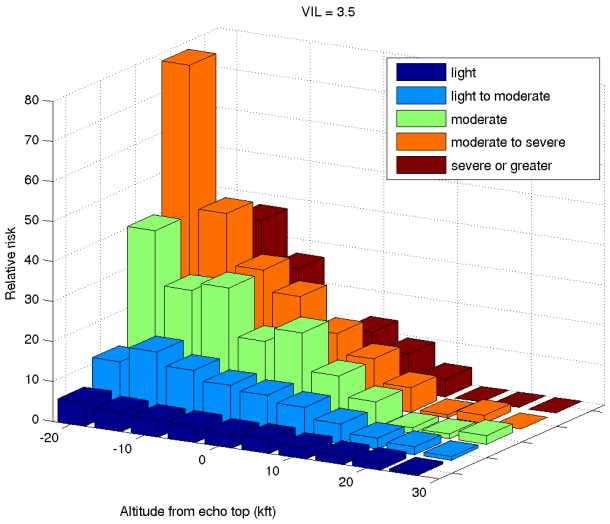

Figure 2: Distribution of vertical proximities to radar echo tops for various levels of turbulence intensity. The *z*-axis is again in terms of "relative risk."

weather radars—called Weather Surveillance Radar 88 Doppler (WSR-88D) or Next-Generation Radar (NEXRAD)—to directly detect turbulence in clouds and thunderstorms that may be hazardous to aviation. The NTDA, which is now part of the NEXRAD Open Radar Products Generator software, is a fuzzy-logic algorithm that uses radar reflectivity, radial velocity, and spectrum width data to perform data quality control and compute eddy dissipation rate (EDR) along with an associated confidence (called EDC). For locations where there is a sufficiently strong radar return (e.g., in clouds and precipitation) and the spectrum width contamination is not too large, the EDC values are close to one and the data may be used with high confidence. Both EDR and EDC are produced for each elevation tilt on a polar grid with 1 degree azimuth and 2 km range spacing. For the past three years, a real-time demonstration of the NTDA has been run at NCAR over increasingly larger domains. The summer 2008 demonstration used data from the 133 NEXRADs depicted in **Error! Reference source not found.**, which cover nearly the entire CONUS. The raw Level II data are obtained in real-time from Integrated Radar Data Services (IRaDS) and ingested using Unidata's Local Data Manager (LDM) software. Each elevation tilt is processed separately, with output produced on a polar grid. Every five minutes, the latest data from each radar in the demonstration domain are merged onto a mosaic grid having 15 vertical levels at intervals of 3,000 ft starting at 3,000 ft. The horizontal resolution of the grid is 0.02° latitude by 0.02° longitude, or approximately 2 km × 2 km. The mosaicking algorithm works by computing the latitude, longitude and mean sea-level (MSL) altitude of each spherical-coordinate radar data point using a standard beam-bending model to account for the refractive index gradient. Each measurement having a confidence above some threshold is then incorporated into a distance- and confidence-weighted average at each nearby mosaic grid point. The distance weighting function used is determined by the volume coverage pattern (VCP) employed by the radar, and is designed to interpolate vertically and use a range-dependent Gaussian-shaped smoothing kernel in the horizontal. Additionally, the height of the maximum radar measurement for each column in the grid is computed. This height field is then smoothed and used as an estimate to the detectable cloud top height. Grid points above the estimated cloud top height are assigned a confidence of zero and are flagged as "bad" data. This last step is useful in mitigating the radar "ring" artifacts that otherwise often appear in the mosaic, particularly at the upper altitudes. In addition, "tops"

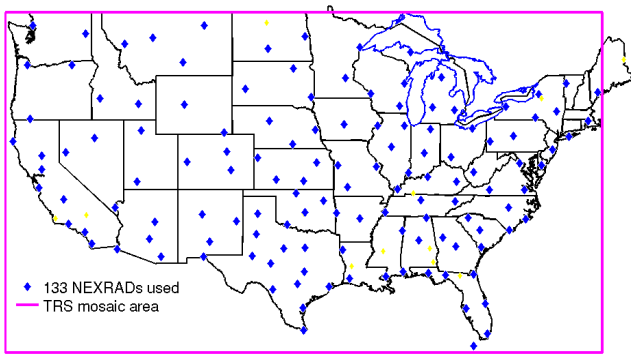

Figure 3: The 133 NEXRADs in the 2008 NTDA demonstration (blue diamonds) and those not used (yellow). Of those not used, only the one in Maine and the one in southern Kentucky have real-time Level II data available.

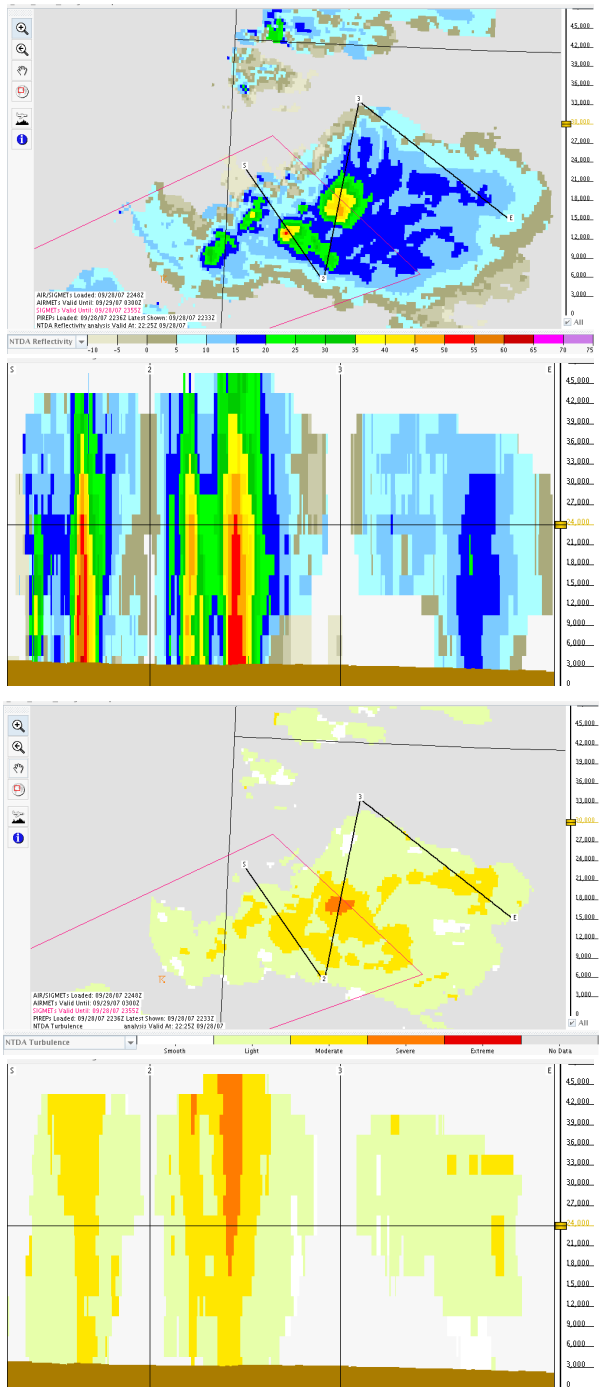

Figure 4: The top two panels show reflectivity (dBZ) in horizontal (30,000 ft. MSL) and vertical cross sections taken along the indicated path through a storm in western Kansas; the bottom two panels depict NTDA-measured EDR for the same cross sections through the same cloud.

products are computed for regions of EDR > 0.1 $m^{2/3}$ s^{-1} (roughly, light or greater turbulence), EDR > 0.3 $m^{2/3}$ s^{-1} (moderate or greater turbulence), and EDR > 0.5 $m^{2/3}$ s^{-1} (severe turbulence). These 2D maps, similar to NEXRAD echo tops products, provide useful summary information regarding the potential in-cloud turbulence hazard.

One interesting aspect of NTDA output is the generally poor correlation of turbulence intensity with reflectivity. An example is provided in Fig. 4, which shows NTDA-computed EDR compared to radar reflectivity. In this case, which is representative, maximum values of EDR are above the rain shaft. Thus for hazard avoidance purposes it is important to realize the distinction between reflectivity (and hazards that may be associated with it, e.g., hail) and turbulence.

c. DCIT

While the NTDA uses Doppler weather radar data to detect in-cloud turbulence hazards, it does not provide turbulence information in regions with low-SNR radar returns, contaminated data or poor radar coverage. Operational NWP models have limited utility in diagnosing regions of out-of-cloud CIT due to latency issues, inadequate model resolution, and incomplete model physics. For these reasons, an FAA and NASA-funded effort is underway to use thunderstorm features derived from various observations along with NWP model data representing the storm environment to infer locations in and around storms where turbulence is likely to exist. The new CIT diagnosis product resulting from this research, called DCIT, will be incorporated into the new GTG Nowcast (GTGN).

The intensity of CIT is related to the size, depth, intensity, longevity and other features of a thunderstorm as well as characteristics of the near-storm environment including stability, strength of upper-tropospheric vertical shear and the interaction of the thunderstorm outflow with ambient winds. Although progress is being made in better understanding the relation of the thunderstorm-environment interaction with CIT, the case studies performed so far are insufficient to systematically or quantitatively characterize these relationships. Thus, empirical models are sought to associate thunderstorm observations and Rapid Update Cycle (RUC; Benjamin et al. 2004) model data with *in situ* reports of turbulence intensity to provide the required diagnostic capability.

Several sources of data are available for providing thunderstorm characteristics and environmental state variables that may be expected to be related to the incidence of CIT. These include 2-D vertically integrated liquid (VIL, kg m^{-2}), NEXRAD echo tops data, GOES satellite imager data and a cloud-to-ground lightning density field derived from the National Lightning Detection Network (NLDN). Near-storm environment data are provided by the RUC NWP model. The RUC data include 13-km 2-D and 3-D grids of variables including winds, turbulent kinetic energy (TKE), convective available potential energy (CAPE), convective inhibition (CIN), potential temperature, humidity mixing ratio, and a number of others. Additionally, all of the RUC-derived turbulence diagnostics used in the GTG forecast algorithm, which was referenced earlier, may be used. These include Richardson number (Ri), structure function eddy

dissipation rate (EDR), horizontal and vertical shear, inverse stability, and a large number of others.

To develop an empirical model relating these quantities to turbulence intensities, each *in situ* EDR measurement collected during some period (June - October 2005 in the results shown below) is associated with collocated feature variables. These include the RUC and RUC-derived data from the closest model analysis time, interpolated from the nearest points surrounding the aircraft location. The GOES IR temperature nearest the point is also used, as is the radar echo top data for the nearest mosaic grid point. The distance to the nearest NCWD VIL value above each of several selected convective intensity thresholds (0.14, 0.76, 3.5, 6.9, 12 and 32 kg m^{-2}) are also computed. These various feature variables do not represent *independent* predictors of turbulence; rather, they are quite highly correlated with one another. The prediction of turbulence must be achieved by an empirical function of the joint distribution of these variables, which can be built using a machine learning data fusion method such as the random forest technique described in Williams et al. 2008. During training, the random forest technique evaluates the importance of each variable (Breiman 2001). Selected results are shown in Table 1. The top two feature variables in the random forest importance list are the GOES channel 4 IR radiance minus the flight level temperature, which is related to the aircraft's vertical position relative to the cloud top, and the GOES IR value itself, which is related to the thunderstorm top's altitude and thus its intensity. The features ranked 3, 4, 6, 9 and 11 are RUC-based turbulence diagnostics that were originally designed to diagnose clear-air turbulence (CAT) but may also include some CIT when the thunderstorm influence is captured by the RUC model forecast. The other top fields are related to the aircraft's horizontal distance to thunderstorm pixels of various intensities. The features ranked 22, 23 and 24 are related to the aircraft's altitude, which in turn is climatologically related to the likelihood of turbulence. Number 25 again reflects the altitude of the aircraft relative to the cloud top, but the NEXRAD reflectivity-based echo top field, which is quantized at 5,000 ft. increments, evidently contributes much less than the GOES IR field to the empirical model's predictive skill.

A prototype DCIT algorithm based on a random forest empirical model is currently running in real-time at NCAR's Research Applications Laboratory, producing both a deterministic EDR estimate as well as probability estimates for light-or-greater, moderate-or-greater and severe-or-greater turbulence derived from the random forest votes. An example screen shot from the research display depicting the probability of moderate-or-greater turbulence is shown in Figure 1. It is clear that many of the flights are navigating around the areas where the probability of turbulence is assessed as high. However, in the case of the flight from eastern Texas into southeastern New Mexico, it appears from the DCIT assessment that the large deviation may be unwarranted given the relatively small threat. Further data collection and verification will be necessary to determine whether the DCIT diagnoses are reliable, and to refine and improve the empirical predictive model.

Table 1: Importance ranks and values for 16 of the top 25 feature fields for diagnosing CIT.

Rank	Impt.	Diagnostic Field
1	3.88	GOES IR minus RUC-derived Flight Level Temp
2	3.43	GOES IR
3	2.80	RUC-derived Structure Function EDR
4	2.60	RUC-derived Ellrod Index
5	1.83	Distance to VIL > 3.5 kg m^{-2}
6	1.77	RUC-derived Saturated Richardson Number
7	1.61	Distance to VIL > 6.9 kg m^{-2}
8	1.57	Distance to VIL > 0.9 kg m^{-2}
9	1.55	RUC-derived Frontogenesis Function
10	1.54	Distance to VIL > 12.0 kg m^{-2}
11	1.47	RUC-derived Vertical Shear
12	1.42	Distance to VIL > 30.0 kg m^{-2}
…		
22	0.78	RUC MSL Pressure minus RUC Flight Level Pre
23	0.76	RUC Pressure
24	0.74	RUC-derived Temperature
25	0.73	NEXRAD Echo Top minus Geopotential Height

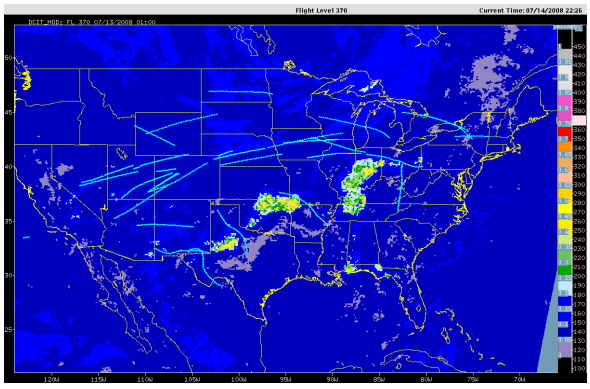

Figure 1: Sample output from a prototype random forest-based DCIT algorithm running in real-time at NCAR/RAL, depicting the estimated probability of encountering moderate-or-greater turbulence at 37,000 ft MSL. Overlaid are United Airlines B-757 flight tracks for aircraft flying between 35,000 and 40,000 ft, some of which are clearly deviating around the regions identified by DCIT as potentially hazardous.

d. Inferences of CIT mechanics based on high-resolution numerical simulation case studies

Thunderstorms can induce major disturbances to their surroundings, including changes in stability, winds and windshear, but the precise mechanisms for the generation and propagation of CIT are not currently well-understood. Fine-scale numerical modeling studies have just begun; nevertheless, these early results point to complicated processes, some of which may be resolvable by current operational NWP, while others cannot. However in unresolvable cases it may be possible to parameterize the relevant CIT generation processes to provide a CIT diagnostic that could be applied to NWP-resolved fields.

1) STUDIES OF ABOVE-CLOUD CIT

CIT above cloud has been a known aviation hazard for many years (Pantley and Lester 1990, Prophet 1970). The generation of gravity waves by convection and their propagation into the stratosphere is well-known (e.g., Fovell et al. 1992, Lane et al. 2001); in a numerical modeling study of a severe turbulence encounter that occurred directly above deep convection, the breakdown of these convectively-induced gravity waves was found to be the most likely explanation for the turbulence (Lane et al. 2003). In the Lane et al. case study, the convectively-induced gravity waves had short periods (10-15 mins), short horizontal wavelengths (5-10 km), and therefore relatively slow horizontal phase speeds (5-15 m/s). Lane et al. showed that when these relatively short scale, high frequency waves propagate vertically in an environment with moderate above-cloud wind shear, the waves can either decrease in amplitude with height, i.e., they are evanescent, or as is well-known (e.g., Booker and Bretherton 1967, Fritts 1982), may interact with a critical level (the level z_c where $U(z_c)-c=0$) and break. Here U(z) is the background wind speed at height z, and $c=\omega/k$ is the wave phase speed where ω is the wave frequency and *k* is the horizontal wavenumber. These processes are summarized schematically in Fig. 6, and the reader is referred to Lane et al. (2003) and Lane and Sharman (2006) for more details. It is the breakdown of the downshear-propagating gravity waves that probably makes the most important contribution to turbulence generation above convection.

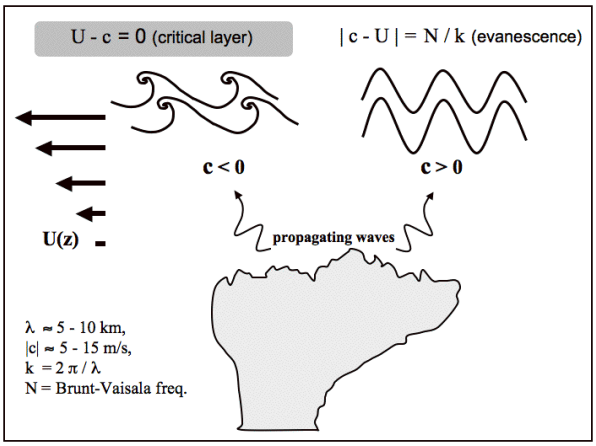

Figure 6. Schematic of gravity wave propagation and breakdown above deep convection in an environment with negative above-cloud wind shear, in a reference frame moving with the cloud top wind. If the change in wind speed is sufficiently large the waves with negative phase speed will encounter a critical layer and break down into turbulence, while the waves with positive phase speeds will become evanescent. Typical values of phase speeds and horizontal wavelengths are shown. (From Lane and Sharman 2008).

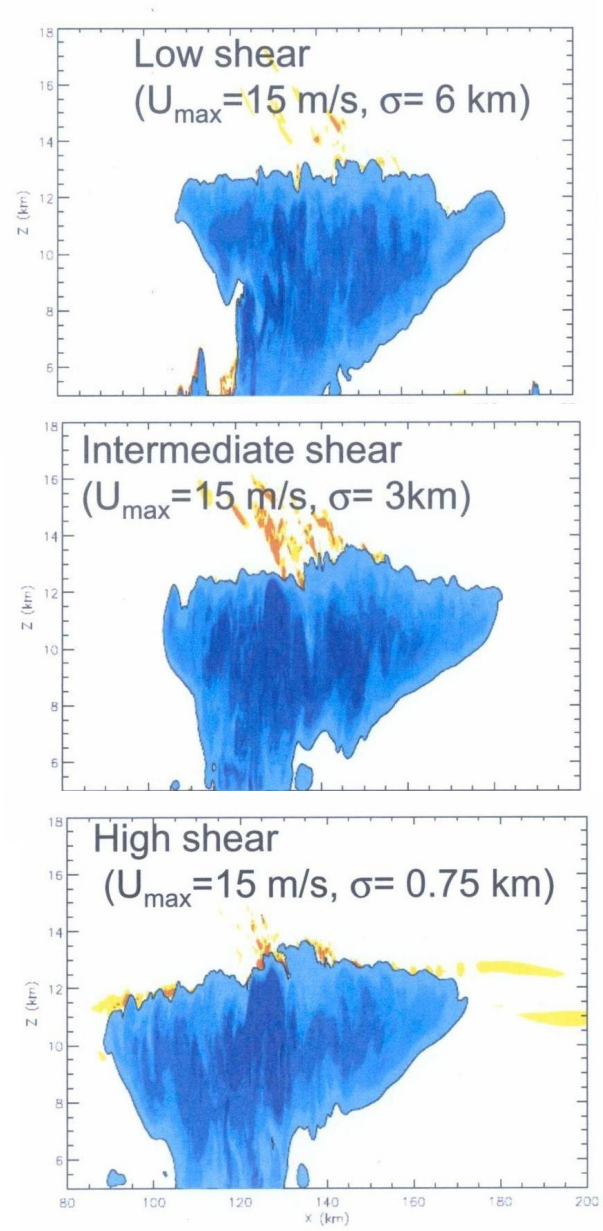

Figure 7. Simulated CIT above cloud for three cases of environmental wind shear with an environmental Gaussian wind speed profile of half-width σ and maximum wind speed Umax at the tropopause height of 12 km. Blue region marks the cloud boundaries and yellow and red indicate levels of modeled elevated turbulence. (Adapted from Lane and Sharman 2008).

The results of Lane et al. (2003) were extended by Lane and Sharman (2008) to include the effects of variations in the strength of the above cloud wind shear and static stability on the breakdown of gravity waves in the lower stratosphere, and the resultant influence of these changes on the extent and intensity of above cloud CIT. Figure 7 shows some influences of the effects of vertical wind shear above the cloud top on the extent and intensity of turbulence above the cloud. Note that the

model-generated turbulence maximizes for intermediate values of the vertical wind shear. Lower values have critical levels too far above the cloud top for wave interaction and breakdown while high values of the vertical shear cause the critical level to be too close to the cloud top for vertically propagating gravity waves to be well-developed. Other simulations where the stratospheric stability Ns was varied showed that decreasing Ns favored CIT above cloud. Thus for these cases CIT likelihood is favored by intermediate values of wind shear and low values of stratospheric stability; neither of these effects is reflected in the current FAA thunderstorm avoidance guidelines.

2) STUDIES OF NEAR-CLOUD CIT

Gravity waves can also be generated by thunderstorms and may propagate laterally away from the storm. If the waves propagate into an already low Richardson number (Ri) environment (low stability and or high vertical wind shear), these waves may further reduce the Ri locally to the point of inducing Kelvin-Helmholtz instabilities and turbulence away from the storm. An example of this effect was provided in the case study of Fovell et al. (2007). This case was identified by reports of moderate to severe turbulence from several *in situ* equipped aircraft at about 0240 UTC on 5 Aug 2005 in the clear air about 20 km to the southeast of an activity thunderstorm cell near the Illinois-Indiana border. Figure 8 shows the observed radar reflectivity compared to the positions of the severe *in situ* turbulence reports (EDR > 0.5 $m^{2/3}$ s^{-1}).

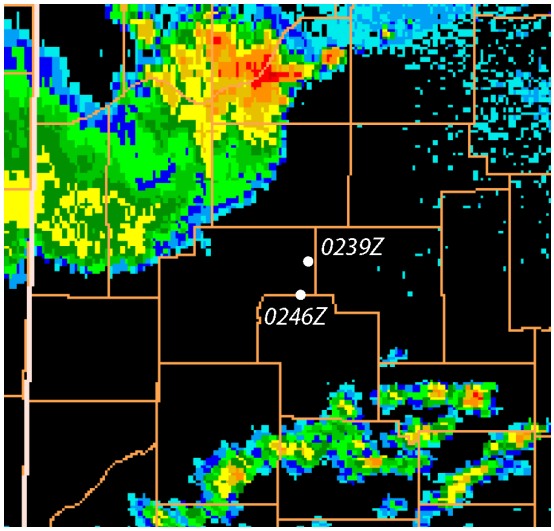

Figure 8: 0244 UTC radar from KIWX, with turbulence report locations identified.

Both "dry" and "moist" WRF (ARW v2.2) model (Skamarock et al. 2005) simulations at 1.5 km horizontal resolution and 100 vertical levels initialized with the RUC13 analyses were executed. The output from the moist run is shown in Fig. 9 as both horizontal and vertical cross sections at 0230 UTC. The simulation did a reasonably good job in reproducing the observed timing and location of the storm. Of particular interest are strong effects of the storm on the upper level wind field and the gravity waves propagating horizontally away from the storm (with a phase speed of about 23 m/s) towards the SE obvious in the vertical velocity field. The vertical cross section also shows reductions in Ri associated with the wave, but it is difficult to know how much of the Ri reduction is due to the presence of the gravity waves and how much is due to other storm-related effects.

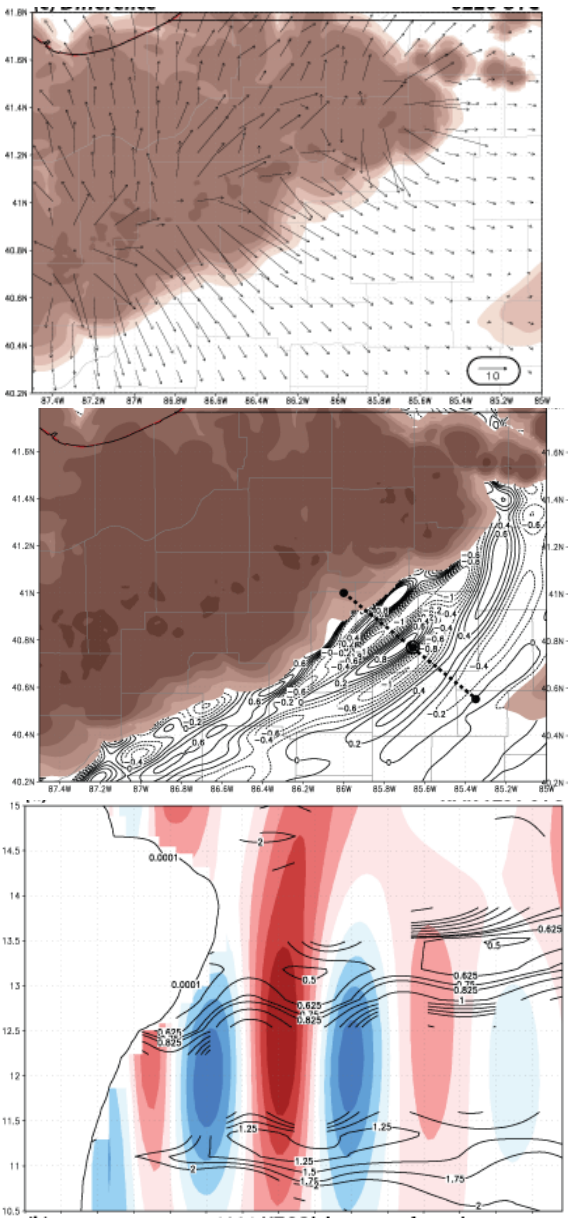

Figure 9. Upper panel: vector wind difference field between the dry and moist simulation. Middle panel: horizontal cross section at 12 km elevation showing the modeled cloud condensate fields (brown) and the vertical velocity field (contour lines). Lower panel: Vertical cross section along the dashed line shown in the upper panel. Vertical velocity is shown as colored contours (red positive, blue negative), and Ri values are contour lines. (Courtesy of Rob Fovell, UCLA.)

Other studies have shown that convective outflow from either isolated thunderstorm cells or large mesoscale convective systems can modify the static stability and vertical shear within the upper troposphere, lowering Ri and producing turbulence in certain locations relative to the convection. One such case was studied in detail by Trier and Sharman (2009). This case was selected because of a continuous trail of moderate turbulence measured by *in situ* equipped aircraft on the northern flank of a Mesoscale Convective System (MCS) over large parts of the middle western states on the nights of 16 and 17 June 2005. Figure 10 shows the *in situ* data reports relative to satellite imagery. The reports were above the anvil, and were far removed from the region of active convection over Oklahoma. Of interest is the coincidence of the elevated turbulence reports in the vicinity of transverse bands emanating from the convection on both nights.

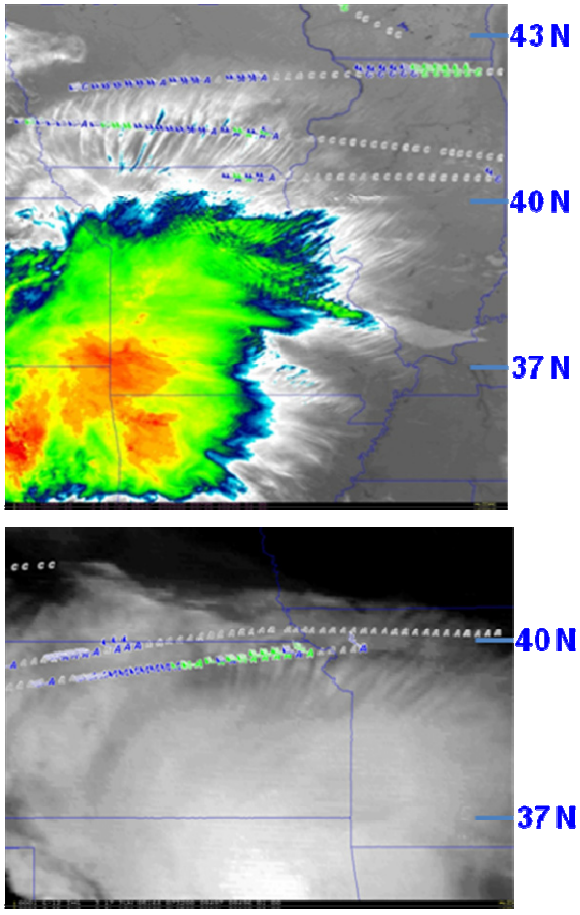

Figure 10. *In situ* tracks overlaid on satellite imagery for 0905 UTC 16 June 2005 (upper) and 0745 UTC 17 June 2005 (lower). Aircraft measured winds and elevated *in situ* values (green-light, blue moderate) are shown on the flight tracks. (Courtesy of Kris Bedka, UW-CIMSS.)

To determine the cause of these CIT encounters, Trier and Sharman ran WRF simulations, both with and without moisture (the "dry" scenario is manufactured by setting the latent heating to zero) for the 17 June case using a horizontal resolution of 3 km and 65 vertical levels. Figure 11 shows the results of model-produced turbulent kinetic energy (TKE) and radar reflectivity compared to the observed reflectivity and elevated turbulence reports after 10.5 hrs of simulation time. The overall agreement of modeled generated reflectivity and regions of elevated TKE is very good, suggesting that the most important factors causing the observed turbulence have been captured.

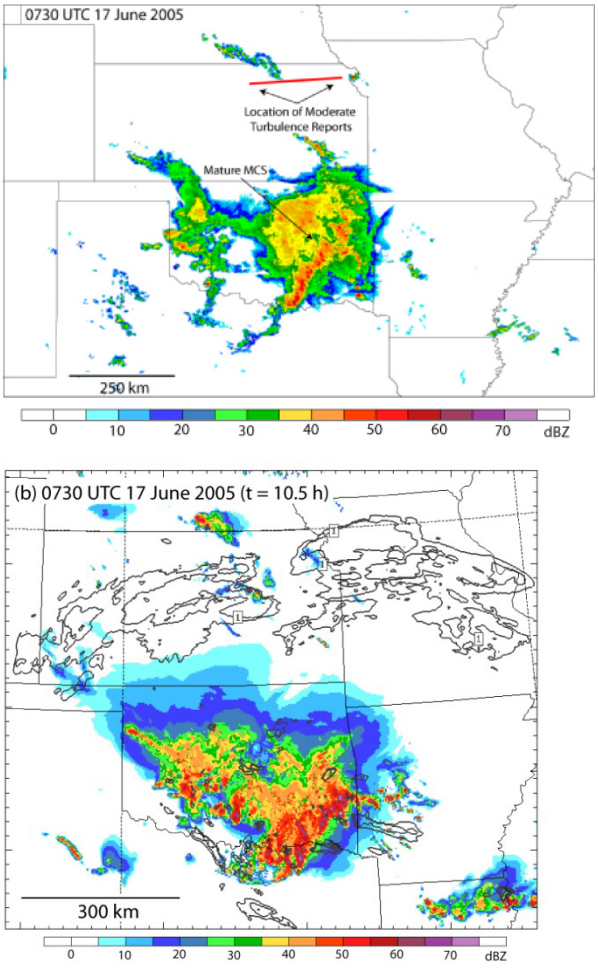

Figure 11. Upper panel: observed radar reflectivity and moderate turbulence reports. Lower panel: modeled maximum radar reflectivity in a vertical column and contours of enhanced TKE (0.5, 1,2,4,8 m^2/s^2 contour intervals) at 11.75 km elevation. (Adapted from Trier and Sharman 2009.)

In this simulation, gravity waves, although present, were only of small amplitude and did not appear to play a significant role in the CIT production. Instead, larger scale effects associated with the convection in the outflow region of the MCS reinforced already strong jet stream winds and led to enhanced shears in the

northern part of the storm. This effect, coupled with stability advection along the outflow, led to significantly reduced Ri to the northeast of the MCS, hundreds of km away from the active convection. After looking at many MCS cases like this, Trier and Sharman concluded that this situation is common, and although the preferred locations of turbulence will depend on the exact alignment of the jet stream with the outflow from the MCS, the schematic shown in Fig. 12 does explain the cause of CIT outside many large scale storms.

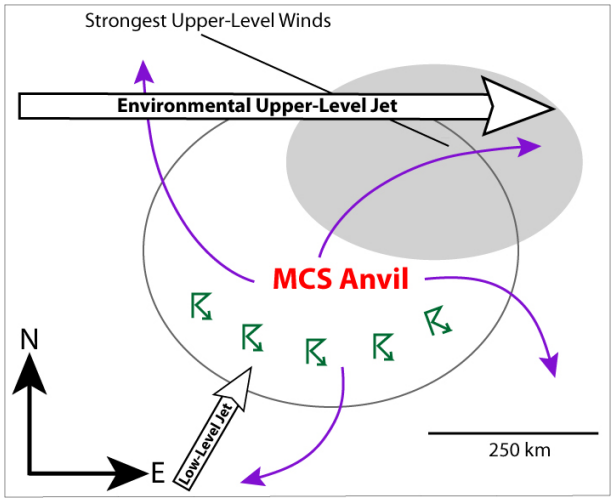

Figure 12. Schematic diagram illustrating spatial relationships among the environmental flow, strongest deep convection (thunderstorm symbols), MCS anvil cloud (thin oval-shaped curve), MCS divergent upper-level outflow streamlines (purple arrows), and the location of strongest upper-level outflow winds (gray shading). (Adapted from Trier and Sharman 2009.)

4. SUMMARY AND FUTURE WORK

The causes of convectively-induced turbulence (CIT) are slowly becoming better understood through the use of high-resolution simulations of observed CIT cases. This enhanced understanding will eventually lead to better turbulence diagnostics that will be exploited in an automated DCIT algorithm. In the meantime, a prototype DCIT algorithm is being developed and tested that uses random forest artificial intelligence techniques to combine available environmental information and turbulence diagnostics derived from a NWP model analysis, radar-based thunderstorm proximity, intensity and coverage data, NEXRAD echo tops, and satellite radiance data to predict the likely location of CIT. A key to DCIT development is the truth data provided by the automated *in situ* measurements which provide accurate training and verification data sets. The NTDA currently provides quantitative estimates of in-cloud EDR, so the NTDA and DCIT algorithms together provide a complete picture of both in-cloud and out-of-cloud CIT.

The relevance of CIT to NextGen is obvious: optimal routing to enhance traffic flow must also account for the turbulence hazard, both within and outside the visible or radar-indicated cloud boundaries. In the future TFM models can ingest the GTGN grids in near real-time to produce the required route structures that maximize the use of air space efficiently while minimizing encounters with turbulence hazards.

Future work will involve continued testing and evaluation of the DCIT and GTGN products, continued simulations of CIT events to obtain a more comprehensive understanding of the CIT phenomenon, and, finally integrating GTGN into TFM automated tools.

5. ACKNOWLEDGEMENTS

The DCIT/GTGN project involves contributions from various scientists and engineers and NCAR and other institutions. We gratefully acknowledge the contribution of our collaborators: Gary Blackburn, Steve Carson, Larry Cornman, Andy Cotter, Jason Craig, Stan Trier, Gerry Weiner, Jamie Wolff and Jaimi Yee (NCAR), Rob Fovell (UCLA), Wayne Feltz and Kris Bedka (U. of Wisconsin-Madison SSEC CIMSS), John Mecikalski (U. of Alabama-Huntsville) and Todd Lane (U. of Melborne).

This research was funded in part by a NASA Cooperative Agreement Notice award from the Science Mission Directorate's Applied Sciences Program (NASA Grant NNS06AB54A (ref: NNS06AA61A).

This research is in response to requirements and funding by the Federal Aviation Administration (FAA). The views expressed are those of the authors and do not necessarily represent the official policy or position of the FAA.

6. REFERENCES

Benjamin, S. G., G. A. Grell, J. M. Brown, T. G. Sminova, and R. Bleck, 2004: Mesoscale weather prediction with the RUC hybrid isentropic-terrain-following coordinate model. *Mon. Wea. Rev.*, **132**, 473-494.

Booker, J.R. and F.P. Bretherton, 1967: The critical layer for internal gravity waves in shear flow. *J. Fluid Mech.*, **27**, 513-539.

Breiman, L., 2001: Random forests. *Machine Learning*, **45**, 5-32.

Cornman, L. B. and B. Carmichael, 1993: Varied research efforts are under way to find means of avoiding air turbulence. *ICAO Journal*, **48**, 10-15.

Cornman, L. B., C. S. Morse, and G. Cunning, 1995: Real-time estimation of atmospheric turbulence severity from in-situ aircraft measurements, *Journal of Aircraft*, **32**, 171-177.

Cornman, L. B., G. Meymaris and M. Limber, 2004: An update on the FAA Aviation Weather Research Program's *in situ* turbulence measurement and reporting system. *11th AMS Conference on Aviation, Range, and Aerospace Meteorology*.

Fovell, R., D. Durran, and J.R. Holton, 1992: Numerical simulations of convectively generated stratospheric gravity waves. *J. Atmos. Sci.,* **49**, 1427-1442.

Fovell, R. G., R. D. Sharman, and S. B. Trier, 2007: A case-study of convectively-induced clear-air turbulence. Preprints, *12th Conference on Mesoscale Processes*, Amer. Meteor. Soc., Waterville Valley, NH, CD-ROM 13.4.

Fritts, D.C., 1982: The transient critical-level interaction in a Boussinesq fluid. *J. Geophys. Res.,* **87**, 7997-8016.

Kaplan, M. L., A. W. Huffman, K. M. Lux, J. J. Charney, A. J. Riordan, and Y.-L. Lin, 2005: Characterizing the severe turbulence environments associated with commercial aviation accidents. Part 1: A 44-case study synoptic observational analysis. *Meteor. Atmos. Phys.*, **88**, 129-153.

Lane, T.P., M.J. Reeder, and T.L. Clark, 2001: Numerical modeling of gravity wave generation by deep tropical convection. *J. Atmos. Sci.*, **58**, 1249-1274.

Lane, T. P., R. D. Sharman, T. L. Clark, and H.-M. Hsu, 2003: An investigation of turbulence generation mechanisms above deep convection. *J. Atmos. Sci.*, **60**, 1297-1321.

Lane, T.P., and R.D. Sharman, 2006: Gravity wave breaking, secondary wave generation, and mixing above deep convection in a three-dimensional cloud model, *Geophys. Res. Lett.*, **33,** L23813, doi:10.1029/2006GL027988.

Lane, T. P., and R.D. Sharman, 2008: Some Influences of Background Flow Conditions on the Generation of Turbulence due to Gravity Wave Breaking above Deep Convection. *J. Appl. Meteor. Climatol.*, **47**, 2777–2796.

Pantley, K.C., and P.F. Lester, 1990: Observations of severe turbulence near thunderstorm tops. *J. Appl. Meteor.*, **29**, 1171-1179.

Prophet, D.T., 1970: Vertical extent of turbulence in clear air above the tops of thunderstorms. *J. Appl. Meteor.*, **9**, 320-321.

Sharman, R. D., L. Cornman, J. K. Williams, S. E. Koch, and W. R. Moninger, 2006a: The AWRP Turbulence PDT. *12th AMS Conference on Aviation, Range, and Aerospace Meteorology*, 3.3.

Sharman, R., C. Tebaldi, G. Wiener and J. Wolff, 2006b: An integrated approach to mid-and upper-level turbulence forecasting. *Weather and Forecasting*, **21**, 268-287.

Skamarock, W. C., J. B. Klemp, J. Dudhia, D. O. Gill, D. M. Barker, W. Wang, and J. G. Powers, 2005: A description of the Advanced Research WRF version 2. NCAR Tech. Note TN-468+STR, 88 pp. [Available from NCAR, P. O. Box 3000, Boulder, CO 80307.]

Trier, S. B. and R. D. Sharman, 2009: Convection-permitting simulations of the environment supporting widespread turbulence within the upper-level outflow of an MCS. To appear in *Mon. Wea. Rev*.

Williams, J. K., R. Sharman, J. Craig and G. Blackburn, 2008: Remote Detection and Diagnosis of Thunderstorm Turbulence. In W. Feltz and J. Murray, Eds., *Remote Sensing Applications for Aviation Weather Hazard Detection and Decision Support. Proceedings of SPIE*, 7088, paper 708804.

Wolff, J. and R. Sharman, 2008: Climatology of upper-level turbulence over the continental Unites States. *J. Appl. Meteor. Climatol.,* **47,** 2198-2214.